[UCI]I804:48009-200000002406

Master of Science

SCALE EFFECTS OF SOLID-GAS INTERACTION ON GAS PRESSURE IN NANOCHANNEL

The Graduate School

of the University of Ulsan

School of Mechanical Engineering

Zhonghua Wang

Scale Effects of Solid-Gas Interaction on Gas Pressure in Nanochannel

Advisor: Dr. Kim BoHung

A Master's Thesis

Submitted to the Office of Graduate School of
University of Ulsan
in partial Fulfillment of the Requirements for the Degree of

Master of Science

by

Zhonghua Wang

School of Mechanical Engineering

Ulsan, Republic of Korea

December 2017

Scale Effects of Solid-Gas Interaction on Gas Pressure in Nanochannel

This certifies that the master's thesis

of Zhonghua Wang is approved by

_____

Committee Chair Dr. Kyoungsik Chang

_____

Committee Member Dr. Jichul Shin

_____

Committee Member Dr. BoHung Kim

School of Mechanical Engineering

Ulsan, Republic of Korea

December 2017

ABSTRACT

Scale Effects of Solid-Gas Interaction on Gas Pressure in Nanochannel

By

Zhonghua Wang

Chair of Advisory Committee: Prof. Kyoungsik Chang

December 2017

A large number of micro-devices involving fluid flow in microstructures have been designed and produced in the late 1980s. As the microscale and nanoscale electromechanical systems (MEMS and NEMS), energy direct conversion technology, microfluidics and nanofluids, quantum structures and components, electronics, photonics and optoelectronics, molecular sensing and biomedical diagnosis of nano-materials as well as the development of scanning probe microscopy techniques to explore energy in micro-/nano scale transport mechanism is also becoming increasingly important. Understanding the energy transfer mechanism of micro-/nano-scale is significant for development of nanotechnology. When the characteristic length can be compared to the length of the mechanical, the continuity hypothesis in traditional thermal analysis may be broken. However, even in such cases, the continuum description breaks down on the nano-material interfaces. Therefore, we present the result of our investigations using Molecular Dynamics (MD) simulations with continuum equations, analyze the feasibility of the simulation results and check the validity and limitations of the continuum hypothesis.

In the Chapter II, we provide the basic theoretical background, especially the difference between ideal gas and real gas, and show the calculation method (derivation) for gas pressure. In Chapter III, the MD simulation technique and the system model to be simulated are described, including a description of the simulation domains and a summary of the simulation parameters. Besides, I explain the stress tensor computations and methods used in MD algorithm. In Chapter IV, I did the feasibility analysis for gas pressure of simulation results through the control of the variable method. Furthermore, I verified that the state of simulated fluid is gas by Radial Distribution Function (RDF) analysis. In Chapter V, simulation results obtained on gas pressure profile and density distribution are shown and discussed subsequently for a system in thermal equilibrium. Finally, in Chapter VI, I provide a comprehensive conclusion about the work presented in this thesis.

DEDICATION

For my beloved family

ACKNOWLEDGEMENTS

I would like to express my sincere gratitude to my academic advisor, Prof. BoHung Kim, for the continuous support of my research over the past two years. His excellent guidance, caring, patience provided me in all the time of research and writing of this thesis. I have learned many things since I became Dr. Kim's students. I greatly appreciate him as my advisor. Without his passionate participate and input, I could not have imagined finishing my research within two years successfully.

During the period of two years, many friends are helpful to color my life. I would also like to thank all the members of Micro/Nano-Scale Thermo-Fluids Engineering Laboratory for their assistances in many aspects that I cannot list them all due to limited spaces. It has been a wonderful experience for me to work and play with them, and they helped me in numerous ways during two years.

Last but not least, I owe more than thanks to my whole family members. Especially, I want to thank parents for their support and love they gave me during the passing years. Also, I want to thank my elder brother for always believing in me and encouraging me with his best wishes. Without their support, it's very hard for me to finish my graduate education.

TABLE OF CONTENTS

ABSTRACT i

DEDICATION iii

ACKNOWLEDGEMENTS iv

TABLE OF CONTENTS v

LIST OF FIGURES vii

LIST OF TABLES ix

I. INTRODUCTION 1

II. THEORETICAL BACKGROUND AND CALCULATION METHOD 7

2.1. Difference Between Ideal and Real Gas 7

2.1.1. Kinetic Theory of Gas 7

2.1.2. Real Gas: Deviations from Ideal Behavior 8

2.2. Theoretical Derivation of Gas Pressure 8

2.3. Micro-/Nanoscale Fluid Mechanics 9

2.3.1. Mean Free Path 9

2.3.2. Knudsen Number 10

III. MOLECULAR DYNAMIC SIMULATIONS DETAIL 13

3.1. Molecular Dynamic (MD) Method 13

3.1.1. Introduction 13

3.1.2. Simulation Setup 15

3.1.3. Practical Various Parameters 19

3.2. Simulation Models and Parameters Setting 21

3.2.1. Simulation Models 21

3.2.2. Simulation Parameters Setting 22

3.3. Calculation Method of Gas Pressure....24
3.3.1. IK Pressure Expression....24
3.3.2. Simulation Methods on Pressure....26
IV. FEASIBILITY ANALYSIS FOR GAS PRESSURE....29
4.1. Radial Distribution Function (RDF)....29
4.2. Kinetic and Virial Components of Pressure Distribution....31
V. RESULTS AND DISCUSSIONS....35
5.1. Comparison of Pressure Profile....35
5.2. Density Distribution....37
5.3. Pressure Distribution....42
VI. CONCLUSIONS....46
REFERENCE....49

LIST OF FIGURES

Figure 1.1. Experimental evidence of micro-devices involving fluid flow: Overview of microfluidic chip design and the method of patterning hydrogels by capillary pinning. (a) A photograph of the microchip with attached tubing. (b) A zoomed in optical microscopy image of the PDMS pillar array (grey) (c) The pillar array with Caco-2 cells (on culture day 8), and culture media filled channels (pink) (d) Schematic isometric view of the microchip with hydrogel patterns[31] 2

Figure 1.2. The smart wall model with linear Couette flow: Density profiles for Kn=10 flow in 5.4nm (a) and 10.8nm (b) height channels; Velocity profiles in Kn=10 flow for 5.4nm (a) and 10.8nm (b) height channels, and the predictions from the Boltzmann equation solutions [16] 5

Figure 3.1. Experimental evidence of liquid water uptake into a nanoscale capillary tube by using MD simulation [43].....14

Figure 3.2. The variation of the Lennard-Jones potential (in units of) and the corresponding forces (Attractive and Repulsive term) as a function of the intermolecular distance [41] 17

Figure 3.3. Schematic and dimensions of simulation domain.....22

Figure 4.1. Profile of the relative density near the wall as a function of the distance to the wall for various gas densities. For the gas-gas interactions the LJ potential is used with (Radial Distribution Function).....30

Figure 4.2. Comparison of bulk pressure in sys1 (a) comparison between IGL, NIST and MD simulation (b) the pressure difference between MD simulation and IGL 32

Figure 4.3. Kinetic and Virial components of local pressure distribution.....33

Figure 5.1. Average pressure profile: (a) the comparison of pressure in sys1, sys2 with variable interaction and 'WCA' potential (b) the relationship between intermolecular interaction and the average pressure 36

Figure 5.2. The relative number density profile each bin (a) the comparison of number density in sys1 and sys2 with variable interatomic interaction (b) partial magnification of number density in sys2 with variable interaction.....38

Figure 5.3. The relationship between number density and interatomic interaction (a) peak number density near the solid wall with variable interaction (b) bulk number density in relatively stable field with variable interaction.....41

Figure 5.4. (a) The pressure distribution in sys1 and sys2 with variable interaction and two-dimensional MD gas flow simulations with the solid wall using the (1,1,0) plane (b) The partial magnification of pressure distribution each bin in sys1 and sys2.....43

Figure 5.5. The relationship between pressure and interatomic interaction (a) peak pressure value near the solid wall under variable interaction (b) bulk pressure in relatively stable field with variable interaction 44

LIST OF TABLES

Table 1. The Units of Style “Metal” in LAMMSP 19

Table 2. Molecular parameters used for solid walls in sys2 23

Table 3. Variable molecular number density of gas flow domain 23

Table 4. Intermolecular interaction parameters utilized in the simulations 24

CHAPTER I

INTRODUCTION

In the past twenty years, microelectronics, micro-fabrication technology, MEMS (micro-electromechanical systems), NEMS (nano-electromechanical systems), quantum structures (such as super-lattices, nanowires, nanotubes, nanoparticles), optoelectronics and lasers, including ultrafast lasers and imaging techniques from molecular to atomic level (such as electron microscopy with high resolution, scanning tunneling microscopy (STM), atomic force microscopy, near-field optical microscopy and scanning thermal microscope) and so on have great development.

A large number of micro-devices involving fluid flow in microstructures have been designed and produced in the late 1980s. For example: micro-sensors, actuators, valves, heat pipes and microchannel used in heat exchangers [28-30]. The study of micro/nano fluid is an active field in biomedical diagnosis (chip lab), drug delivery, MEMS/NEMS sensors and actuators, micro-pumps in ink-jet and microchannel heat-sink in electronic cooling are main application field. Many researchers are also studying the flow of fluids in nanostructures (such as nanotubes) and are developing unique devices such as nanojets. There is one application related to the microstructures as shown in blow [31]. The microfluidic cell culture platform was developed to enable long-term cell culturing in periodic 3D compartments under controlled fluid flow.

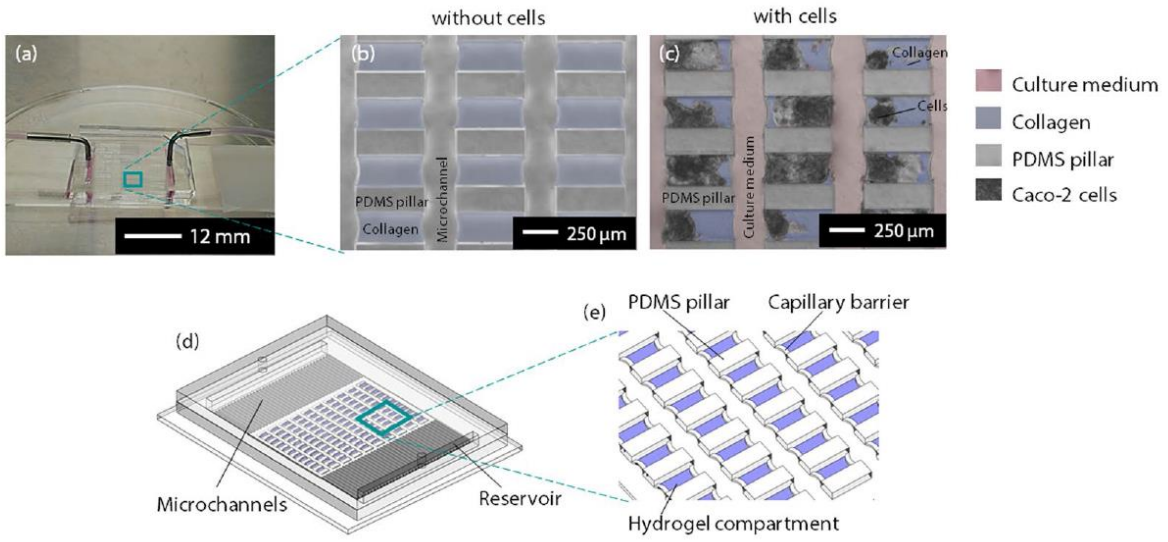

Figure 1.1 Experimental evidence of micro-devices involving fluid flow: Overview of microfluidic chip design and the method of patterning hydrogels by capillary pinning. (a) A photograph of the microchip with attached tubing. (b) A zoomed in optical microscopy image of the PDMS pillar array (grey) (c) The pillar array with Caco-2 cells (on culture day 8), and culture media filled channels (pink) (d) Schematic isometric view of the microchip with hydrogel patterns[31]

In recent years, this field is rapidly shifting to the scale expansion and systems engineering to explore the possibilities of nano-technology and nano-engineering recombinant technologies. When the characteristic length can be compared to the length of the mechanical, the continuity hypothesis in traditional thermal analysis may be broken. Similarly, when characteristic time and mechanical time scales are comparable, the traditional balance method may no longer be suitable for the present research situation. Understanding the energy transfer mechanism of micro-/nano-scale is significant for development of nanotechnology.

The results indicate that the classical transport theory, i.e., Lucas-Washburn equations, fails to predict the fluid rise in such nano conduits [32]. Under the condition of continuity

hypothesis, the objects are continuous and can be divided indefinitely. If the element is designed much larger than the microstructure size of the fluid, but far smaller than the size of the macro device, the mean value of these elements is defined as a parameter.

The mean free path of fluid molecules in micro-/nano-structures may be equivalent to or less than their characteristic dimensions. Because the interaction between the molecules and the solid surface becomes very important, the continuity hypothesis is no longer valid. For example, in Qian's pioneering paper, he attracted the attention of aerodynamics to non-continuous hydrodynamics applications in high altitude flight and vacuum system, and then formed the rarefied gas dynamics [33]. Based on the mean free path characteristic length ratio, that is the Knudsen number, he divided several areas from the traditional gas dynamics (i.e., continuous flow category) in the same article: slip flow, "blank flow" (later called the transition flow) and free molecular flow.

In recent years, in thermal physical engineering, more and more research results about the micro-nano scale constantly emerged, and the timely dissemination of the latest research results is of great significance to the future research. The fluids in the nanochannel can exhibit substantially different physics from what is observed in larger-scale systems because of the breakdown of the continuum hypothesis as well as the increased influences of the wall-force field effects.

In 2005, J Toth et al. investigates the wall-force field can induce adsorption of gas, liquid or dissolved solids onto a surface [24]. In 2011, Murat Barisik et al. studied for fluid behavior within nanoscale confinements. And this conclusion has reinforced the previous results that the interfacial anisotropy primarily induced by the surface-particle virial term and because of the

density layering, an additional wall effect induced by the wall-force field [10]. In addition, they reported the Kn dependency of the surface influence in 2011 and proved the significant influence of wall force field effects in nanoscale confinements [17]. Beyond that, in another study, the authors expressed the fluid behavior in the wall force penetration region depends mostly on the properties of the surface-gas pair by validating independency of the near-wall fluid behavior on channel dimension and flow dynamics in 2014 [3]. In 2016, Jafar Ghorbanian et al. utilize non-equilibrium MD simulations to investigate the scale and wall force field effects for liquid argon flows in nanoscale periodic domains and in nanochannels. Similarly, the results reveal that the deviation from the continuum solution is due to the wall effect [12]. However, gas fluid flows spend much memory requirements of MD simulation. Thus, Murat Barisik et al. utilized the smart wall model to investigate the properties of gas fluid [16]. In this simulation model, the author presents the velocity and density profiles by utilizing the potential strength for gas/wall interactions to be the same with that of gas/gas molecular interaction. The results as shown in below:

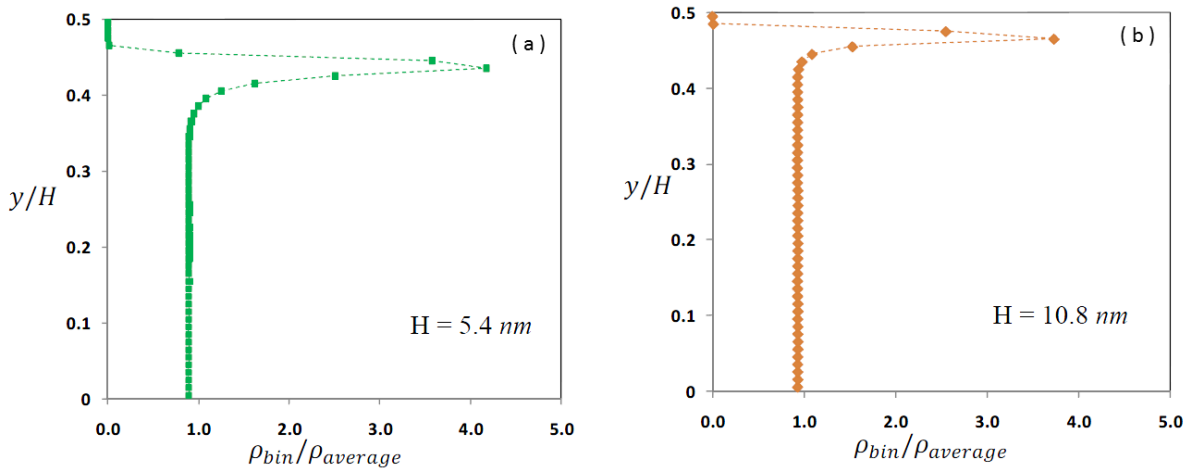

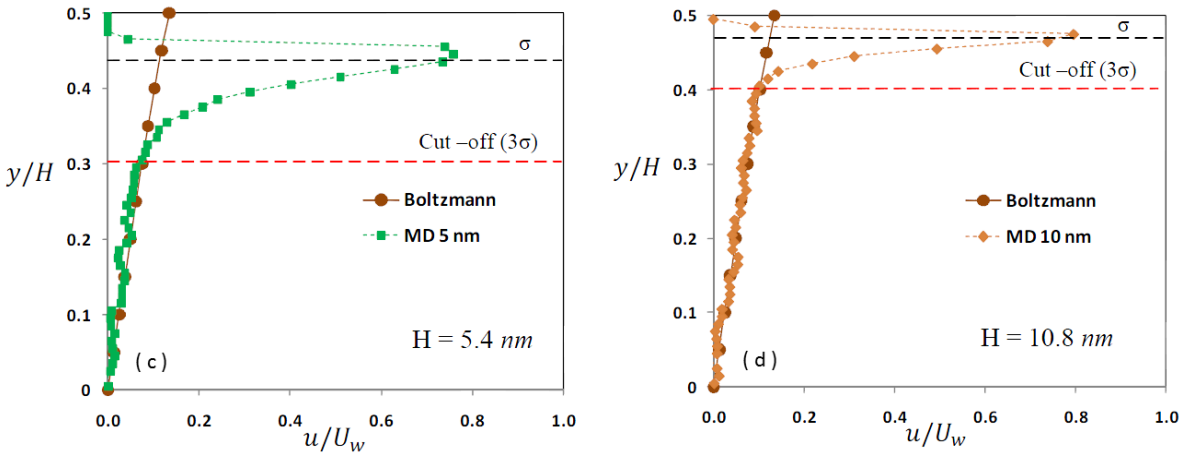

Figure 1.2 the smart wall model with linear Couette flow: Density profiles for Kn=10 flow in 5.4nm (a) and 10.8nm (b) height channels; Velocity profiles in Kn=10 flow for 5.4nm (a) and 10.8nm (b) height channels, and the predictions from the Boltzmann equation solutions [16]

The increasing importance of computational experiments has been recognized since the chemistry Nobel was awarded for the first time to three modelers (K. Karplus, M. Levitt and A. Warshel) in 2013. Computer modelling has become an equal partner with experiments as joining together descriptions of molecules at close-up and zoomed-out scales **[**34**]**. Therefore, in this thesis, I present the result of investigations using molecular dynamics (MD) simulation method and check the validity of the continuum hypothesis. The nanoscale gas flow behavior was analytically solved. In addition, I clarified the contribution of interface effects, especially the influence of near-wall field.

Specifically, I performed equilibrium molecular dynamics simulations using LAMMPS to investigate how fluids behave at interfaces and how the interfacial fluid properties affect fluid transport [35]. Molecular dynamics (MD) simulation packages solve Newton's second law of motion for each atom. The equation of motion is usually integrated within the cut-off distance, with the random initial configurations and initial velocities computed from the Boltzmann

distribution [36]. The trajectory of each atom and thermodynamic properties are obtained from the simulation. By analyzing these outputs, the physical properties of system can be derived. Certainly, these results help to get a better understanding of the fluid behaviors at the interface.

The main goal of this study is to investigate the difference of gas pressure in bulk and near-wall regions of simple fluids in virtual box with or without solid walls. This thesis is organized as follows. In Chapter II, I provide the basic theoretical background, especially the difference between ideal gas and real gas, and show the calculation method (derivation) for gas pressure. In Chapter III, the MD simulation technique and the system model to be simulated are described, including a description of the simulation domains and a summary of the simulation parameters. Besides, I explain the stress tensor computations and methods used in MD algorithm. In Chapter IV, I did the feasibility analysis for gas pressure of simulation results through the control of the variable method. Furthermore, I verified that the state of simulated fluid is gas by Radial Distribution Function (RDF) analysis. In Chapter V, simulation results obtained on gas pressure profile and density distribution are shown and discussed subsequently for a system in thermal equilibrium. Finally, in Chapter VI, I provide a comprehensive conclusion about the work presented in this thesis.

CHAPTER II

THEORETICAL BACKGROUND AND CALCULATION METHOD

2.1. Difference between Ideal Gas and Real Gas

2.1.1. Kinetic Theory of Gas

Kinetic theory of gases based on a simplified molecular or particle description of a gas. The simplest kinetic model is based on the assumptions that:

(1) The gas is composed of a large number of identical molecules moving in random directions, separated by distances that are large compared with their size;

(2) The molecules undergo perfectly elastic collisions (no energy loss) with each other and with the walls of the container, but otherwise do not interact. It means that the force of attraction or repulsion between gas molecules is zero;

(3) The gas particles occupy a negligible fraction of total volume of gas system.

These simplifying assumptions bring the characteristics of gases within the range of mathematical treatment. Such a model describes a ideal gas and is a reasonable approximation to a real gas, particularly in the limit of extreme dilution and high temperature. For example, real gas has less volume than ideal gas at lower pressure, and gas molecules are moving quickly at high temperature.

Based on the kinetic theory, pressure on the container walls can be quantitatively attributed to random collisions of molecules the average energy of which depends on the gas temperature. The ideal gas pressure can therefore be related directly to temperature and density.

2.1.2. Real Gas: Deviations from Ideal Behavior

The behavior of real gases usually agrees with the predictions of the Ideal Gas Law. At low temperature or high pressure, real gas derivate significantly from ideal gas behavior. Actually, the two most important influencing factors are negligible volume and intermolecular interactions. In order to correct for the fact that the pressure of a real gas is smaller than expected from the ideal gas equation, the Van der Waals equation introduces two parameters as modification ideal gas equation to redefine the pressure of real gas:

$$[p + \frac{an^2}{V^2}](V - nb) = nRT \tag{2.1}$$

This equation provides a much better fit with the behavior of real gas than the ideal gas equation. At the same time, this modification equation is very helpful to understand the difference between ideal gas and real gas.

2.2. Theoretical Derivation on Gas Pressure from Energy

As we known, the pressure is defined as a force applied per unit area: $p = F / A$. After a simple transformation, we can express the pressure as the formula of energy to facilitate the subsequent analysis of this study.

$$p = \frac{Force}{Area} = \frac{F \cdot d}{A \cdot d} == \frac{W}{V} = \frac{Energy}{Volume} = \frac{PE + KE}{Volume} \tag{2.2}$$

Here, from the above formula, the computations of the stress tensor components for an atomistic system have two additive components. The first is the kinetic contribution from throughput of linear momentum resulting from the particle velocities, whereas the second contribution is the

potential term, which is an internal contribution from intermolecular forces between the particles. In our simulation, this result has played a decisive role in our study of pressure analyzing. In addition, the kinetic contribution is controlled by the system temperature, while the potential contribution is controlled by the intermolecular interaction. As to this research, it depends largely on the molecular number density.

2.3. Micro-/Nanoscale Fluid Mechanics

2.3.1. Mean Free Path

The mean free path is defined as the average distance traveled by particles between two collisions, which is a very important concept. It is often used to determine whether a given phenomenon belongs to the category of macroscopic scale (continuous), or microscopic scale deduced from the control equation after the local equilibrium hypothesis. One of the applications is in microfluidics field, and the other applies to the conduction of electricity and heat in solid field.

If it is assumed that a particle with a diameter d moves at an average velocity, v (assuming all other particles are stationary). Therefore, the collision frequency, that is, the number of colliding particles per unit time is $\pi n d^2 v$. The time τ between two collisions is the reciprocal of the collision frequency. The mean free path Λ is the average distance between two successive collisions, which is equal to the ratio of the average velocity to the collision frequency. Therefore,

$$\Lambda = v\tau \approx \left(\pi n d^2\right)^{-1} \tag{2.3}$$

It depends only on the particle size and number density. The average time τ between two collisions is called relaxation time, and the average collision frequency τ^{-1} is called the scattering rate or the collision rate. The scattering rate refers to the average number of collisions of individual particle per unit time.

When the relative motion of the particle is investigated based on Maxwell velocity distribution, for the ideal gas:

$$\Lambda \approx \frac{1}{\sqrt{2}\pi n d^2} = \frac{k_B T}{\sqrt{2}\pi d^2 p} \tag{2.4}$$

Scattering rate (or collision frequency) is

$$\tau^{-1} = v / \Lambda \tag{2.5}$$

Here, the relaxation time τ is an important characteristic time. It shows how long the system is restored to equilibrium (local equilibrium at least) after being disturbed.

2.3.2. Knudsen Number

When the characteristic length L_c is equal to the mechanical dimensions (such as mean free path Λ), the continuity model will no longer be established.

This situation occurs when the gas pressure is very low (rarefied gas), or with a much smaller characteristic sizes, several nanometers from a few microns to the micro/nano channel, the continuity model is no longer valid. As a result, the boundary scattering becomes significant, and the probability of collision between gas molecules and wall surfaces will be greater than that of collision between the gas molecules.

The ratio of mean free path to characteristic size defines a very important dimensionless parameter, called Knudsen number

$$Kn = \frac{\Lambda}{L_C} \tag{2.6}$$

Since the Reynolds number and the Mach number are $\mathrm{Re}_L = \rho v_\infty L_C / \mu$, $Ma = v_\infty / v_a$ respectively. Where, v_∞ is the free flow velocity; $v_a = \sqrt{\gamma RT}$ is the velocity of sound in the gas. When considering internal flow, v_∞ is replaced by the overall velocity v_m. So,

$$Kn = \sqrt{\frac{\pi\gamma}{2}} \frac{Ma}{\mathrm{Re}_L} \tag{2.7}$$

The physical properties of the flow depend on the size of the Kn. Local Kn determines how rarefied the fluid is and how far it deviates from the continuity hypothesis [44]. Lower Kn usually corresponds to the continuous flow (Kn ≤ 0.001), in this region, the Wiener-Stokes equation is applicable, the velocity of the fluid at the boundary is same as the velocity at the surface, in addition, the temperature of the fluid near the surface is same with the temperature at the surface. Non-continuous (slip) boundary conditions must be used when Kn increases from 0.001 to 0.1.

If $\mathrm{Kn} \geq 10$, the flow is called free molecular flow, and the ballistic scattering between the molecules and the surface is dominant. The continuity assumption is completely ineffective, and it cannot define local velocity or temperature of fluid, "slip" velocity is equal to the mainstream velocity. That is, regardless of the distance from the wall, the velocity of the fluid is same. Same case for the temperature of fluid, even there is heat transfer between the wall and the gas, there is

no temperature gradient near the wall. Based on the molecular models, such as BTE or DSMC, it is the best way to solve this problem in this region and in the transition flow region between the slip flow and free molecular flow [37].

CHAPTER III

MOLECULAR DYNAMIC SIMULATIONS DETAIL

3.1. Molecular Dynamics (MD) Method

3.1.1. Introduction

Molecular dynamic is a computer simulation technique where the time evolution of a set of interacting particles is followed. This is done by numerically solving the equations of motion (Newton's Law) of classical multibody systems. Given the positions, masses and velocities of all particles in the system and the forces on the particles, the motion of all (individual) particles can be followed in time by calculating the (deterministic) particle trajectories. We used molecular dynamics code LAMMPS (Largescale Atomic/Molecular Massively Parallel Simulator) to simulate the gas flow.

In MD simulation, the first step is initialization, which randomly distributes the N molecules in the spatial region and set their velocity according to a certain equilibrium distribution. After the initial statistical allocation, all the remaining steps are deterministic. The temporal evolution of each particle's position and velocity can be obtained by integrating the values of the Newton's motion equations with a short time step. Periodic boundary conditions are generally used to simulate the inlet and outlet of the fluid. Statistical averages, also known as ensemble averages, can be used to calculate the internal energy, effective temperature, pressure, and other parameters within a given period of time. The internal energy is the sum of all kinetic energy and potential energy, and the temperature is calculated based on the average kinetic energy (for gas with single atom). The pressure can be calculated by the Virial Theorem [38]. In general, the simulated timestep is the order of femtosecond, and in the real process of simulating

(usually within a few picoseconds), it takes tens of thousands of timesteps. In the process of simulation, the computational time is proportional to the square of the number of particles N. Therefore, after consuming a large amount of computational cost, the MD simulation method can provide all particle trajectory of complete information.

This method is most suitable for very small volume containing the dense gas, liquid and solids that contain amounts of particles. The MD method is particularly applicable in nanostructures because the number of particles becomes relatively small and the overall timestep is manageable easily. It can also be used to simulate boiling and vaporization as well as ablation process. It is noteworthy that, in the study of some nanoscale phenomena, MD method is often the only feasible method because these experiments cannot be carried out. As shown in Fig. 3.1, MD simulation was used to investigate the nanoscale capillary imbibition.

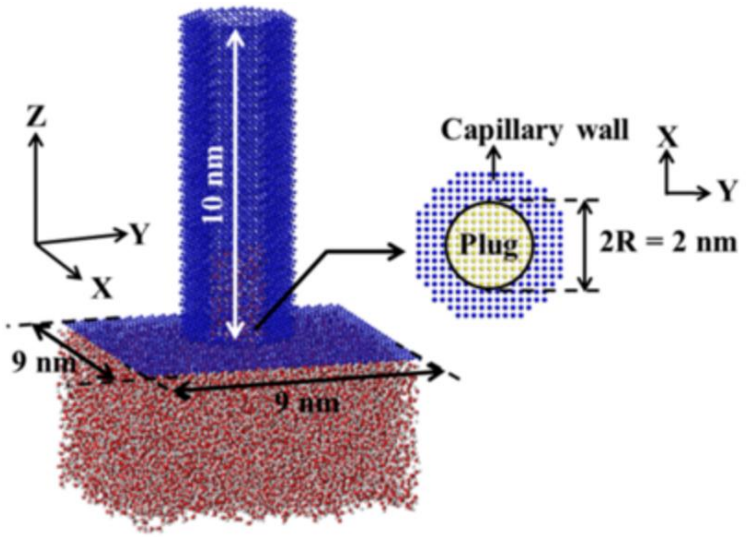

Figure 3.1 Experimental evidence of liquid water uptake into a nanoscale capillary tube by using MD simulation [43]

3.1.2. Simulation Setup

3.1.2.1. Intermolecular Potentials

The definition of accurate intermolecular potentials is the key to MD simulation. In general, the potential energy (V) of a system consisting of N interacting particles can be expressed as:

$$V = \sum_i V_1(r_i) + \sum_i \sum_{j>i} V_2(r_i, r_j) + \sum_i \sum_{j>i} \sum_{k>j>i} V_3(r_i, r_j, r_k) + \cdots \quad (3.1)$$

Where, r_i is the position of particle i. the first term on the right hand side (V_1) is the potential energy due to the external fields, and the remaining terms, which are modeled by intermolecular potentials, represent the particle interactions (e.g., V_2 is the potential between pairs of particles and V_3 is the potential between particle triplets and so on [39])

In many atomistic simulations, it is sufficient to use the simplest models to represent the essential physics, and much pairwise potential have been proposed. Here, I provide some types of potential energy used in my MD simulation.

Lennard-Jones Potential

Lennard-Jones potential is one of the most widely used potentials for nonpolar molecules [40]. The general form of a Lennard-Jones potential is

$$V(r) = \varepsilon \left[\frac{m}{n-m} x^{-n} - \frac{n}{n-m} x^{-m} \right] \quad (3.2)$$

Where, n and m are constants, $x = r / r_m$, and r_m is the separation corresponding to minimum potential energy. The "hard-sphere" diameter is related to the energy-minimum separation r_m by

$$\sigma = r_m \left(\frac{m}{n} \right)^{\frac{1}{n-m}} \tag{3.3}$$

The most common form of the Lennard-Jones potential is obtained when $n = 6$ and $m = 12$, i.e.,

$$V(r) = 4\varepsilon \left[\left(\frac{\sigma}{r} \right)^{12} - \left(\frac{\sigma}{r} \right)^{6} \right] \tag{3.4}$$

The first term in equation (3.4) represents a short-range repulsive force, which prevents overlap of the atoms, while the second term represents an attractive interaction. Fig. 3.2 shows the variation of the Lennard-Jones potential and the corresponding force ($F = -\nabla_r V(r)$). The advantage of the Lennard-Jones potential is that it combines a realistic description of the intermolecular interaction with computational simplicity.

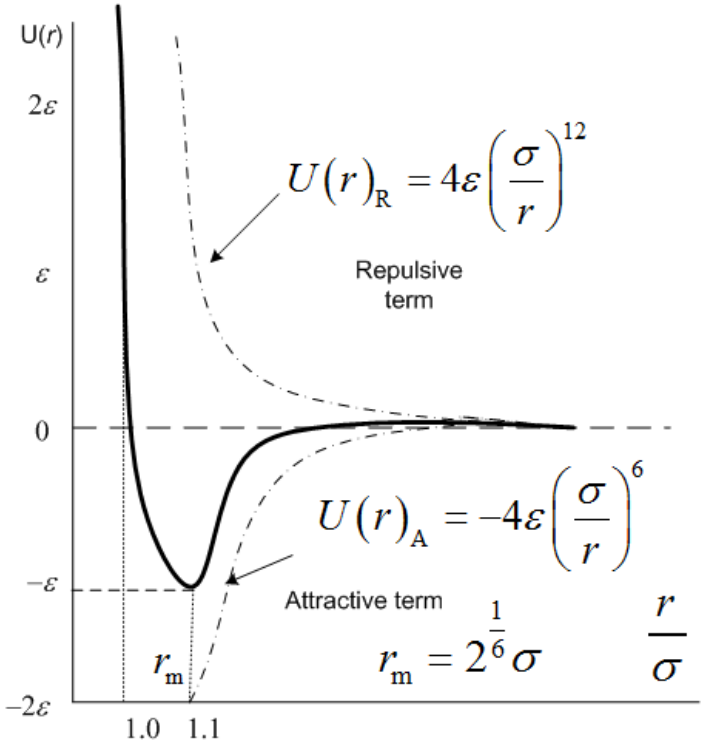

Figure 3.2 The variation of the Lennard-Jones potential (in units of ε) and the corresponding forces (Attractive and Repulsive term) as a function of the intermolecular distance [41]

WCA Potential

The WCA (Weeks-Chandler-Andersen) potential is a modification of the Lennard-Jones potential, where the atoms interact via a cut and shifted Lennard-Jones interatomic potential function defined by

$$V(r) = \begin{cases} 4\varepsilon\left[\left(\frac{\sigma}{r}\right)^{12} - \left(\frac{\sigma}{r}\right)^{6}\right] - V_{LJ}(r_c), & r \le r_c \\ 0, & r > r_c \end{cases} \qquad (3.5)$$

Where, r_c $(=\sigma/2^{1/6})$ is the truncation distance, V_{LJ} (r_c) is the value of the Lennard-Jones potential at the point of truncation, and σ and ε are the Lennard-Jones distance and energy

parameters. In this case, the interactions between the atoms are purely repulsive. Therefore, this potential is used in this research which I want the atoms to purely repel each other.

3.1.2.2. Common Statistical Ensembles

Am ensemble is a collection of points in phase space satisfying the conditions of a particular thermodynamic state. Several ensembles, with different constraints on the thermodynamic state of the system, are commonly used in MD. It is very important concept of statistical mechanism, which is the basis of almost every statistical property. For example:

NVT ensemble

The canonical ensemble is a collection of all system whose thermodynamic state is characterized by a fixed number of atoms, N, a fixed volume, V, and a fixed temperature, T. generally, the NVT system could be thought like a system transport heat with an infinity heat source. It is an appropriate choice for the models with periodic boundaries and the energy or the pressure or the volume but not when the temperature needs to be calculated from the simulation.

NVE ensemble

The micro-canonical ensemble has a thermodynamic state characterized by a fixed number of atoms, N, a fixed volume, V, and a fixed energy, E. this corresponds to and isolated system.

NPT ensemble

The NPT ensemble (also known as the isobaric-isothermal ensemble) is characterized by a fixed number of atoms, N, a fixed pressure, P, and a fixed temperature, T.

3.1.2.3. Units in LAMMPS

There are several types of units for different simulation system. The related command determines a series of units of all quantities specified in the input script and data file, as well as quantities output file. In my research, the style of units was set "*metal*", main units was shown in blow:

Table 1 the Units of Style "Metal" in LAMMSP

Mass	grams/mole	
Distance	Angstroms, Å	1.0 Angstrom = 1e-10 meters = 0.1 nm
Time	picoseconds, ps	1.0 ps = 1e-12 s = 1e+3 fs
Temperature	Kelvin, K	T(K) = T(℃) + 273.15
Force	eV/Angstroms	
Energy	eV	1 eV =1.602e-19 J = 4.1841.602e-19cal
Pressure	bars	1 bar = 1e+5 pascals

3.1.3. Practical Various Parameters

Size of the Time Step

We would like to use as large as a timestep as possible so that we can explore more of the phase space of the system. However, the timestep needs to be small enough so that the Taylor's series expansions can provide a reliable estimate of the atomic positions and velocities at the end of the timestep. A good way to check the whether the timestep is small enough is to run an

equilibrium simulation without temperature coupling. If the fluctuation in the total energy is less than 0.5% of the total energy of the system, the timestep is typically acceptable.

Cut-Off Scheme

The most expensive part of energy and force calculations is the nonbonded interactions, since there are $N(N-1)/2$ such interactions to calculate in an N-atom system. To save computer time, it is usual practice to neglect nonbonded interactions that occur between atoms separated by more than a given distance (say 10Å). This use of a cut-off scheme in potential/force calculation is justified for potentials like the Lennard-Jones potential. However, for charged atoms, the use of a cut-off scheme is not easily justified: charge-charge interactions are of much longer range (because of the $1/r$ dependence of the interaction energy).

Boundary Conditions

The most commonly employed boundary conditions in MD are the periodic boundary conditions. The atoms of the system to be simulated are put into a space-filling box, which is surrounded by translated copies of itself. Thus there are no boundaries of the system; the artifact caused by unwanted boundaries in an isolated cluster is now replaced by the artifact of periodic conditions.

Freezing a Group of Atoms

Atoms that are supposed to remain stationary can be frozen to reduce the computational time. This is useful during equilibration.

Number of Bins

In the binning method, the system is partitioned into cells. The total number of cells or the size of the individual cell is an important choice. Since we want to estimate a certain variable, which varies continuously in space, a larger number of bins mean a finer grid and thus a better estimation. The choice of the number of bins also depends on the parameter that needs to be extracted.

3.2. Simulation Models and Parameters Setting

3.2.1. Simulation Models

In this study, two systems were simulated to investigate the gas behavior respectively. The schematic diagram of the simulation domain was shown in Fig. 3. Except the solid walls in Fig. 3(b) (system 2), all of the simulation environment parameters are same. In Fig. 3(a), the system1 was built in a virtual box to compare the difference of argon properties obtained by calculating (Ideal Gas Law) and MD simulation. The original crystal structure is Face-Centered Cubic (FCC).periodic boundary conditions were applied in three directions. The system2 was shown in Fig. 1(b). The gas flow is confined between two solid walls which are a distance H = 4nm apart. Copper walls were modeled with FCC crystal structure, and (1, 0, 0) plane faces the gas molecules. And the original gas lattice crystal included 3 λ x 5 λ x 2 λ unit cells with FCC structure.

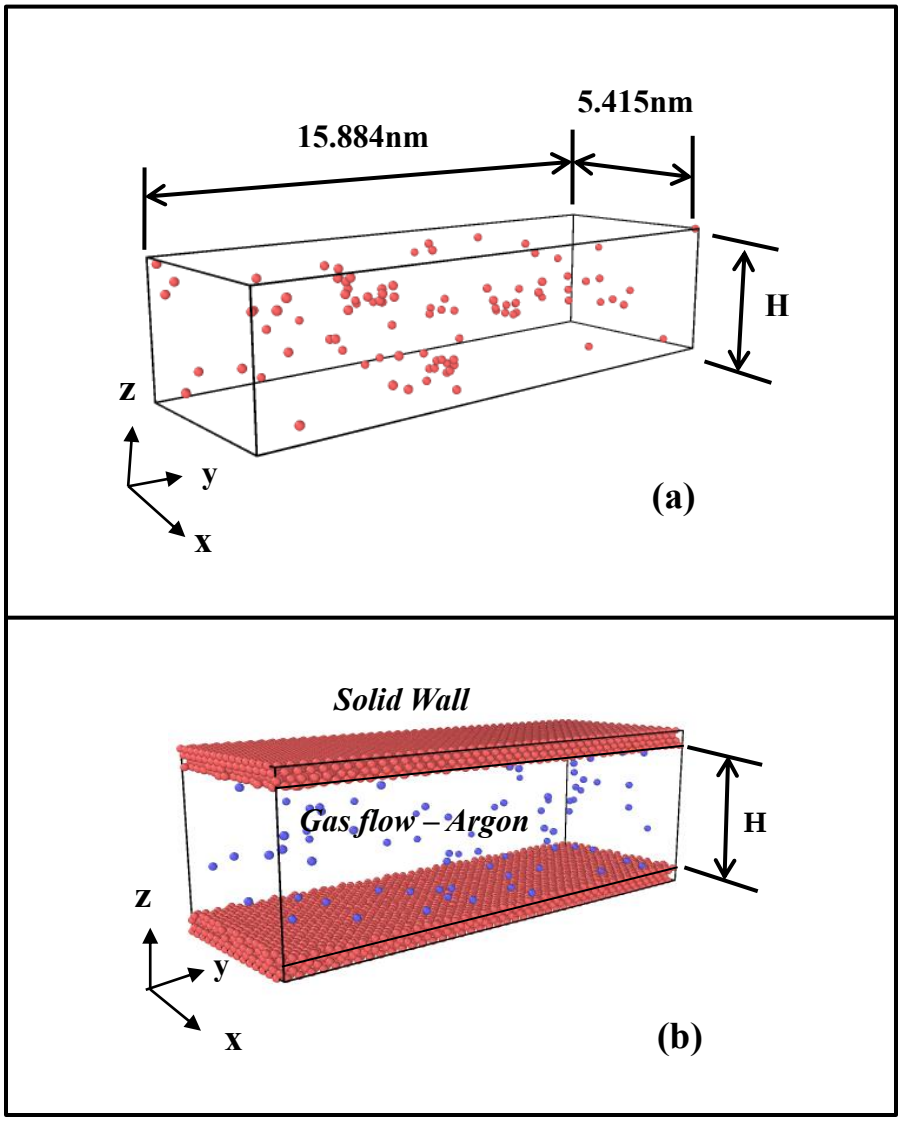

Figure 3.3 Schematic and dimensions of simulation domain

3.2.2. Simulation Parameters setting

In this study, periodic boundary conditions were applied in x and y axis directions. In addition, the molecules parameters of solid walls in system2 were illustrated in Table 2.

Table 2 Molecular parameters used for solid walls in sys2

Wall	Mass(g/mol)	Lattice Constant(Å)	Number of molecules for each wall	Number of wall layers
Cu	63.546	3.61	5280	4

All simulations were performed at 300K temperature and number density varying from 0.28 to 0.42 (Table 3).

Table 3 Molecular number density of gas flow domain

Case #	Number density, ρ_N	Number of argon molecules
1	0.281938	97
2	0.325537	112
3	0.418547	144

The molar mass for an argon molecule is M = 39.948002g/mol, its molecular diameter is σ_{Ar} = 3.405 Å, and the depth of the potential well for argon is ε_{Ar} = 0.0103eV. For simplicity, the same molecular characteristic length was utilized for wall molecules, so the gas flow was simulated with Kn = 10 (Knudsen number).

In this study, a cut-off distance 1.0 nm was applied. The intermolecular interaction parameters between gas-gas and solid-gas molecules were shown in Table 4. Although it's impossible to actual material due to the changes in gas-solid interaction. However, we can change the interaction between solid and gas molecules trough some chemical treatments. Thus we can achieve the purpose of this study and realize the uneven gas distribution. Meanwhile, the embedded atom method (EAM) was utilized to model the interatomic forces between the FCC

copper due to its accurate description of the total energy through consideration of embedding energy as a function of atomic electron density. [27] Besides, Weeks-chandler-Andersen (WCA) potential simulation was used to investigate the pressure profile in sys2.

Table 4 Intermolecular interaction parameters utilized in the simulations

solid-gas interaction	**$\varepsilon_{Ar\text{-}Ar}$(eV)**	**$\varepsilon_{Cu\text{-}Ar}$(eV)**
0.001 ε	0.0103	6.50E-05
0.005 ε		3.25E-04
0.01 ε		6.50E-04
0.05 ε		3.25E-03
0.1 ε		6.50E-04
0.2 ε		1.30E-02

The simulation domains were divided into 400 slab bins for temperature and density profiles in order to observe the gas behaviors in the vicinity of the solid surfaces. The simulation time step (r) was set to 1.0 fs. The molecular dynamics code Large-scale Atomic/Molecular Massively Parallel Simulator (LAMMPS) was used for all MD simulations in this study. The isothermal ensemble (NVT) (i.e., constant mole, N, volume, V, and temperature, T) was used to establish equilibrium systems. All simulations were performed for 2.0 ns.

3.3. Calculation Method of Gas Pressure

3.3.1. IK Pressure Expression

As shown in before, we know the derivation of pressure by two part, kinetic energy and potential energy. Therefore, we have to explain two components respectively. For the kinetic part, the gas behavior is likely the ideal gas. So the kinetic part of pressure can be obtained by the Ideal Gas Law.

$$p = \frac{p_{xx} + p_{yy} + p_{zz}}{3} = \frac{1}{3V} mv^2 \tag{3.6}$$

As to the potential component of pressure, we have to introduce the Virial Theorem [15]. The virial theorem is a powerful tool in the determination of intermolecular forces, and is used directly in the development of an equation of state. Its derivation starts from Newton's equation of the movement direction of a particle of mass m_i, acted upon by a force F_i in the x direction:

$$(F_i)_x = m_i \frac{d^2 x_i}{dt^2} \tag{3.7}$$

It can be written as

$$\frac{1}{2}(x_i F_i)_x = \frac{1}{2} m_i x_i \frac{d^2 x_i}{dt^2} = -\frac{1}{2} m_i (\frac{dx_i}{dt})^2 + \frac{1}{2} \frac{d}{dt} (m_i x_i \frac{dx_i}{dt}) \tag{3.8}$$

Then we have to make the integration for second term in right side of the equation over a sufficiently long time interval τ, as the $\tau \to \infty$,

$$\frac{1}{2} \frac{d}{dt} (m_i x_i \frac{dx_i}{dt}) = \frac{1}{\tau} \int_0^{\tau} \frac{d}{dt} (\frac{1}{2} m_i x_i \frac{dx_i}{dt}) dt = 0 \tag{3.9}$$

Hence, the time average of Eq. (3.8) becomes:

$$-\frac{1}{2} \overline{(x_i F_i)_x} = \frac{1}{2} m_i \overline{(\frac{dx_i}{dt})^2} = \frac{1}{2} m_i \overline{v_i}^2 \tag{3.10}$$

Similar can be written to describe the motion in the y and z directions. Adding the three equations of the form of Eq. (3.11), we can get,

$$-\frac{1}{2}\sum_i \overline{r_i F_i} = \overline{E_k} \tag{3.11}$$

Where, $\overline{E_k}$ is the total average kinetic energy of the system, r_i is the vector position of the particle acted by the force vector F_i. Virial is defined as the expectation value of the sum of the products of the coordinates of the particles and forces acting on them. In a word, total virial for a real gas system equals to the sum of an ideal gas part and a contribution due to interactions between particles.

According to previous ideal Gas Law, the new pressure expression can be derivate. Therefore, to obtain point function stress tensors and pressure profiles, Irving-Kirkwood (IK) pressure expression:

$$p = \frac{1}{3V}\left[\sum_{i=1}^{N}\left\langle m_i \cdot v^2 \right\rangle + \sum_{i=1}^{N-1}\sum_{j=2}^{N}\left\langle \overrightarrow{F_i} \cdot \overrightarrow{r_{ij}} \right\rangle\right] \tag{3.12}$$

It provides a method to calculate local pressure tensors for system based on the equations of hydrodynamics [42]. The IK expression was used at larger separations, attractions predominate, and also at contact molecules repel each other. It was the contribution by kinetic energy and potential energy.

3.3.2. Simulation Methods on Pressure

Two methods were used to compute the "stress" tensor in LAMMPS.

Method 1 – "Compute Stress"

This method can calculate the pressure of the entire system of atoms. The pressure is computed by the formula:

$$p = \frac{Nk_BT}{V} + \frac{\sum_{i}^{N'} r_i \cdot f_i}{dV} \tag{3.13}$$

Where, the N is the number of atoms in the system, k_B is the Boltzmann constant, T is the temperature, and V is the system volume. These second term is the virial, equal to dU / dV, where r_i and f_i are the position and force vector of atom i. The pressure will be output directly by the command: '*compute pressure thermos_temp'*.

Method 2 – "Compute ks + vs"

This method can compute the symmetric per-atom stress tensor for each atom in a group. However, in order to analyze the simulation results intuitively, we will simulate the two components of pressure, kinetic energy and virial energy, respectively and then summarize the results. As below, The formula was used in the simulation:

$$\begin{aligned} S_{ab} = -[mv_a v_b &+ \frac{1}{2}\sum_{n=1}^{N_p}(r_{1a}F_{1b} + r_{2a}F_{2b}) + \frac{1}{2}\sum_{n=1}^{N_b}(r_{1a}F_{1b} + r_{2a}F_{2b}) + \\ &\frac{1}{3}\sum_{n=1}^{N_a}(r_{1a}F_{1b} + r_{2a}F_{2b} + r_{3a}F_{3b}) + \frac{1}{4}\sum_{n=1}^{N_d}(r_{1a}F_{1b} + r_{2a}F_{2b} + r_{3a}F_{3b} + r_{4a}F_{4b}) + \\ &\frac{1}{4}\sum_{n=1}^{N_i}(r_{1a}F_{1b} + r_{2a}F_{2b} + r_{3a}F_{3b} + r_{4a}F_{4b}) + Kspace(r_{ia}, F_{ib}) + \sum_{n=1}^{N_f} r_{ia}F_{ib}] \end{aligned} \tag{3.14}$$

The first term is a kinetic energy contribution for atom l. The second term is a pairwise energy contribution where n loops over the N_p neighbors of atom l, r_1 and r_1 are the positions of the 2 atoms in the pairwise interaction, and F_1 and F_2 are the forces on the 2 atoms resulting from the

pairwise interaction. The third term is a bond contribution of similar fro for the N_b bonds which atom l is part of. There is also a term for the KSpace contribution from long-range Coulombic interactions, if defined. As to the output file, this compute calculates a per-atom array with 6 columns, and we can compute what we want to analyze according to the equation (3.15):

$$
\begin{aligned}
& p_r = p_{r-ks} + p_{r-vs} \\
& = \{-(c\_ks[1] + c\_ks[2] + c\_ks[3]) * Ncount / V_{bin}\} \\
& + \{-(c\_vs[1] + c\_vs[2] + c\_vs[3]) * Ncount / V_{bin}\}
\end{aligned}
\tag{3.15}
$$

CHAPTER IV

FEASIBILITY ANALYSIS FOR GAS PRESSURE

4.1. Radial Distribution Function

One way of quantifying spatial structure is through the use of the radial distribution function g(r) (RDF), which is a measure of the probability that a particle will be located a distance r from a given reference particle. The relative density of atoms as function of radius equals ratio of density of atoms at distance r (in control area dr) by overall density. The radial distribution function is defined as

$$g(r) = \rho(r) / \rho \qquad (4.1)$$

Where, $\rho(r)$ is the local density of atoms, ρ is overall density of atoms (volume). The RDF provides information about the density of atoms at a given radius, also it can indicate what kind of state for the fluid is in system by analyzing the results figure. The figure below shows the function g(r) for the gas and for the liquid argon in system 1.

In Fig. 2, a peak indicated a particularly favored separation distance for the neighbors to a given particle. Thus, RDF revels details about the atomic structure of the system being simulated.

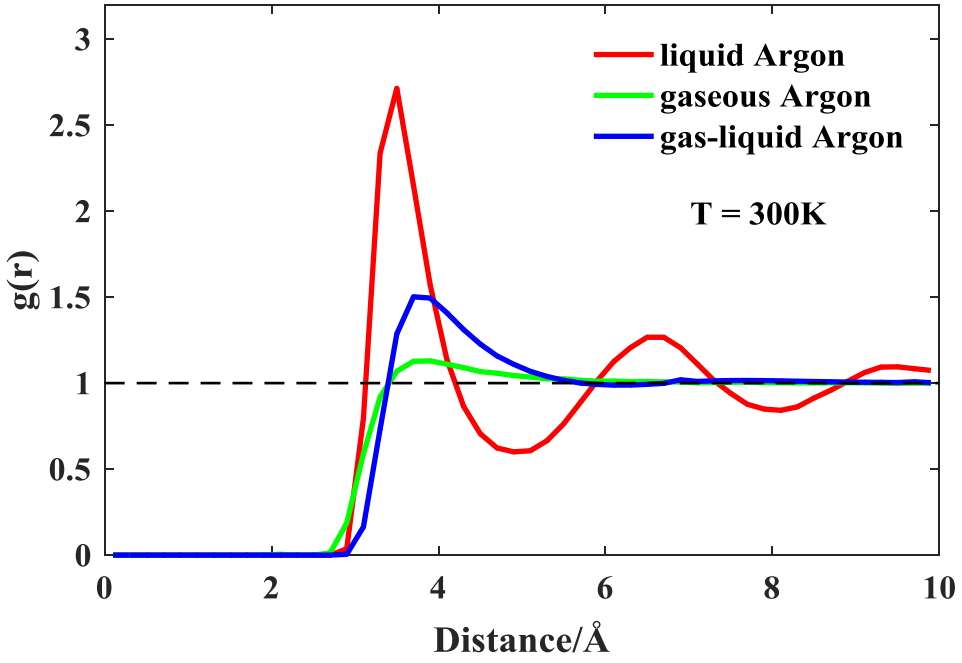

Figure 4.1 Profile of the relative density near the wall as a function of the distance to the wall for various gas densities. For the gas-gas interactions the LJ potential is used with $\varepsilon = 0.0103$ (Radial Distribution Function)

It means, the RDF can distinguish the state of the fluid in simulation system. For the liquid argon system, g(r) exhibits several peaks, indicating that at certain values, it is more likely to find particles than at others. This is a result of the attractive nature of the interaction at such distance. The plot of g(r) also shows that there is essentially zero probability of finding particles at distance less than about 3.0Å from each other. This is duo to the presence of very strong repulsive forces at short distances.

However, gases do not have a regular structure which heavily influences their RDF. The RDF of a real gas will have only a single peak, and then they will rapidly decay to the normal bulk density of gas, $g(r) = 1.0$. Therefore, the simulation results were used to analyze the fluid

state. Since this study is based on the gas pressure, we can ensure that the simulation fluid is valid measurement by the gaseous state.

4.2. Kinetic and Virial Components of Pressure Distribution

Two methods were used in system 1 to get the pressure in results by MD simulation: simulate pressure value directly ('compute stress'), simulate two parts ("compute ks+vs") then calculate the results. Due to almost same simulation results by two ways, one line can be observed clearly in figure 4.2(a). In addition, in order to increase the reliability of results, the NIST experiment data (National Institute of Standards and Technology) was also shown in figure 4.2. Here, the relative deviation ratio n between experiment data and MD simulation result was introduced:

$$n = \frac{P_{Ave,MD} - (P_{Ave,IGL} + (P_{Ave,IGL} - P_{Ave,NIST}))}{P_{Ave,MD}} \tag{4.2}$$

As we know, the most important reason between experiment and simulation is the interatomic potential difference. The LJ potential was used in MD simulation to describe interaction among atoms. However, we know that in real materials the dynamics of atoms is controlled by the laws of quantum mechanics and the bonding is defined by the electrons that are not present in classical MD. Hence, it can be find there exists pressure difference between experiment data (NIST) and simulation (MD). Due to the error between the experiment data (NIST) and calculation of ideal gas (IGL), so we introduce the relative deviation rate to judge the significance of the simulation results. According to the analyzation results, the error value is almost fluctuating at the $n \approx 3.0\%$. Therefore, the deviation ratio is within the allowable range ($n \leq 5.0\%$) and remains constant, so the simulation data is valid and the results are credible.

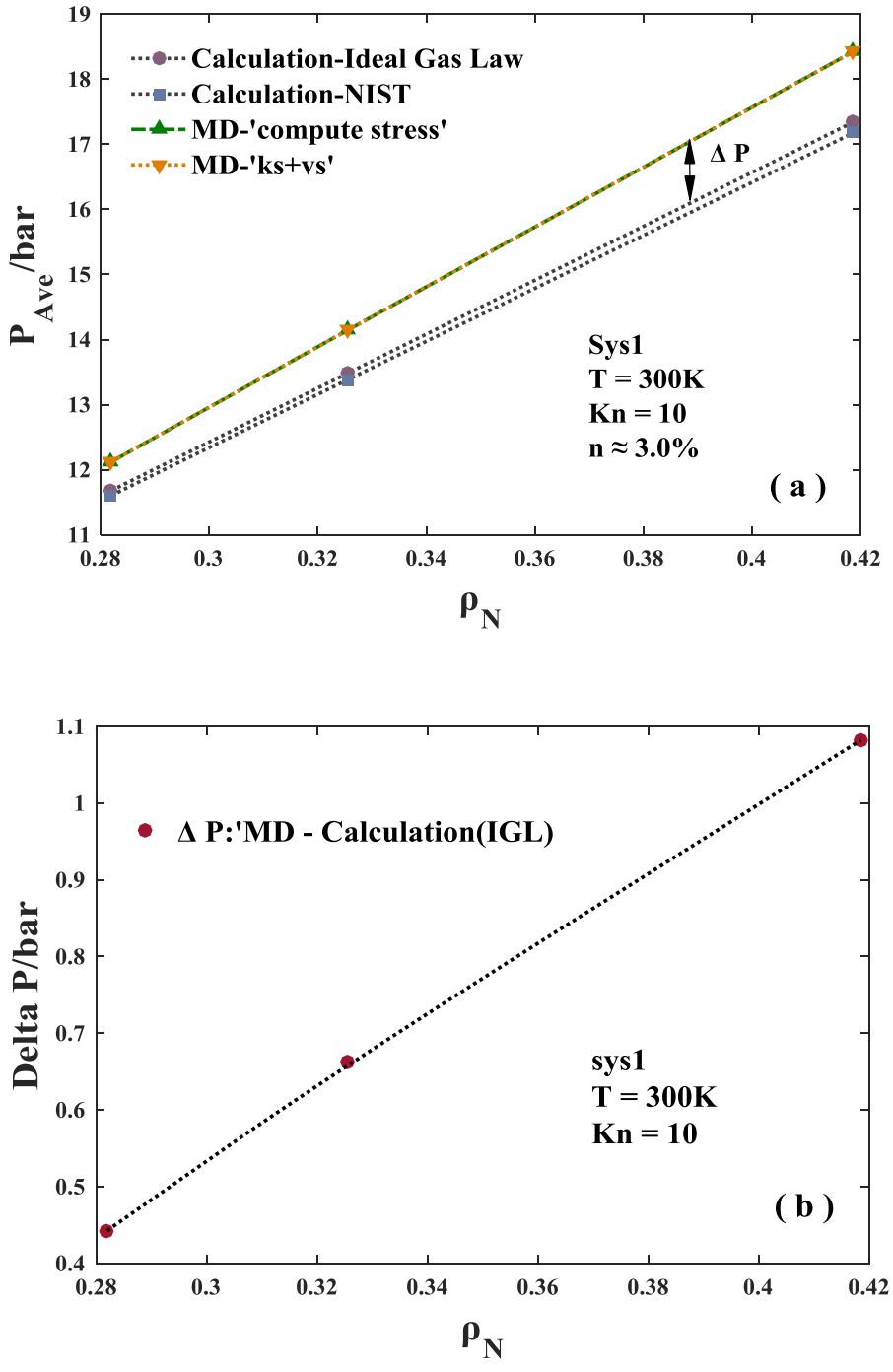

Figure 4.2 comparison of bulk pressure in sys1 (a) comparison among IGL, NIST and MD simulation (b) the pressure difference between MD simulation and IGL

In figure 4.2(a), it can be found a little difference ΔP exists clearly between calculation for ideal gas and simulation for real gas in sys1. And, the difference increases with the increasing the number density due to more and more non-negligible atomic volume (Fig. 4.2(b)). As we know, an ideal gas has three distinct differences from real gas: negligible volume of molecules, elastic collisions with each other and no intermolecular forces except during collision. Particularly, no Van der Waals force between molecules is significant to explain the difference between ΔP. In addition, figure 4.3 will explain this part of difference caused by the virial energy in detail, it can be found clearly the virial part makes contribution to the stress value. So, the data of real gas by MD simulation is higher than ideal gas value by computation.

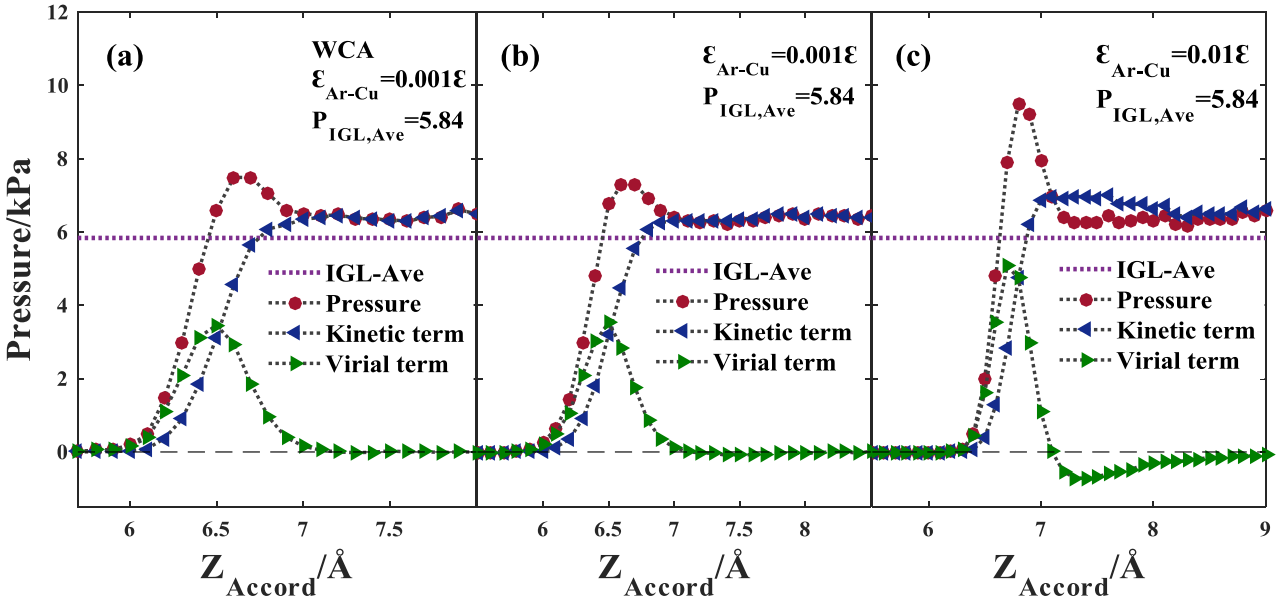

Figure 4.3 Kinetic and Virial components of local pressure distribution (a) WCA potential (b) gas-solid interaction $\varepsilon_{g-s} = 0.001\varepsilon$ (c) gas-solid interaction $\varepsilon_{g-s} = 0.01\varepsilon$

Fig 4.3 demonstrated the pressure variation on $Kn = 10$ flow inside 4.0nm channel as the sum of its kinetic and virial contributions under different gas-solid interaction. The pressure

value is constant in the bulk region and shows variations between 0.68~0.76 nm by WCA simulation. The pressure is defined by the kinetic term in most of the domain, while the surface virial only has a significant effect on the pressure near the wall. For Fig 4.3(b), the virial term data is almost negative but close to zero. However, there exists the negative data clearly while increasing the solid-gas interaction from 0.001epsilon to 0.01epsilon in Fig 4.3(c). Due to the wall force field, more gas molecules were absorbed near the solid wall. Compared the figure 4.3(b) and figure 4.3(c), higher solid-gas interaction, more gas molecules gathered near the solid wall. And that, there is higher kinetic energy and virial energy, it means much higher kinetic term and much lower virial term. As to Fig 4.3(a), the virial part is positive and close to zero due to composing by the repulsive potential in WCA simulation method. However, both repulsive and attractive potential exist in figure 4.3(b), so part of potential energy would be neutralized. In addition, it can be concluded that the pressure simulation results are almost same with each other between sys 1 and sys 2 when the pressure tends to be stable in bulk region.

CHAPTER V

RESULTS AND DISCUSSIONS

5.1. Comparison of Pressure Profile

In this part, all of the data is from MD simulation results and the data obtained by the 'ks+vs' method for pressure simulation. Variable weaker interaction between solid and gas molecules were used to investigate the average pressure in nanochannel. Also, the results of sys1 and sys2 are compared. In addition, Weeks-chandler-Andersen (WCA) potential simulation was also used to investigate the pressure profile in sys2. The Lennard-Jones pair potential is composed into two parts, one entirely repulsive and the other one entirely attractive. However, WCA potential only includes repulsive force. Due to the fixed volume, the comprehensive performance of the molecular force is doing negative work, so the molecular potential energy increases. The average pressure is calculated by the equation below:

$$P_{Ave} = \sum_{bin=1}^{400} \left[(-\sum_{i=1}^{3} pr\_ks\_i)_{bin} + (-\sum_{j=1}^{3} pr\_vs\_j)_{bin} \right] \qquad (5.1)$$

Where, pr_ks_i and pr_vs_j represent the kinetic and virial stress tensor components respectively. Then, sum all of the stress components each bin. According to the calculation results, the Fig. 5.1 is shown below.

In Fig. 5.1(a), the average pressure of variable interaction between Copper and Argon was compared. Beyond that, under almost same environment variables, WCA potential was applied in sys 2 and shown in figure. Also, the average pressure in sys 1 was compared with sys2.

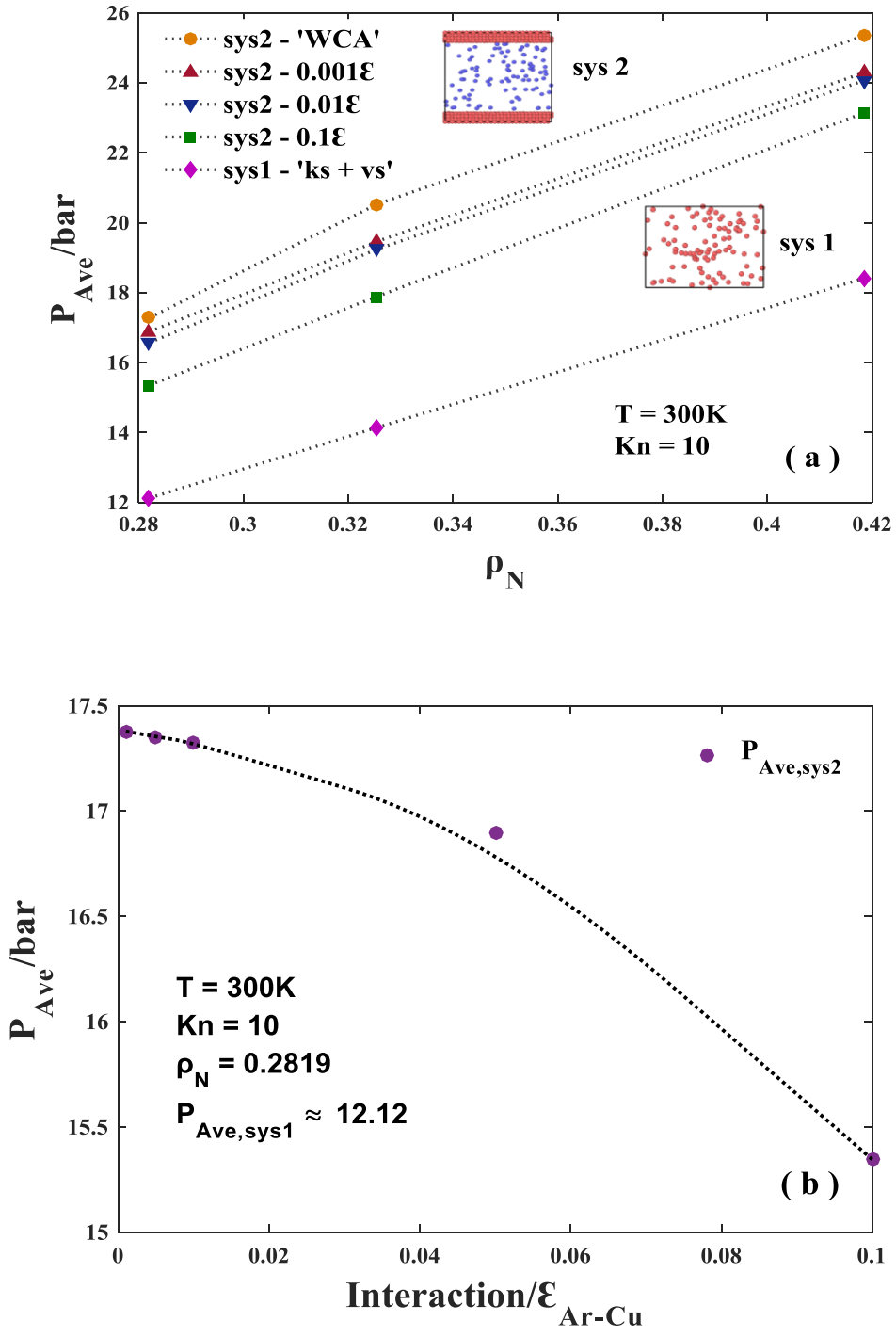

Figure 5.1 Average pressure profile: (a) the comparison of pressure in sys1, sys2 with variable interaction and 'WCA' potential (b) the relationship between intermolecular interaction and the average pressure

It can be clearly observed that the difference in average pressure exists between any groups.

As to sys1 and sys2 with weaker interaction: due to the solid wall, the wall force field was also generated. So, there is a certain amount of gas molecules near the solid wall, and more potential energy was shown in sys2. In the same time, most of the gas molecules are close with each other, so the pressure of potential energy part shows negative value. Therefore, the total pressure value is reduced by the virial part. In addition, from the atomic visualization of sys2, more atoms are gathered closed to the solid wall within 0.1epsilon than 0.001epsilon due to the stronger absorption of wall force field. Therefore, both simulation results explained the significant difference between sys1 and sys2, solid wall, introduces the wall force field. Thus the absorption of wall force field leads part of gas molecules no longer free movement, but rather move closer to the solid wall. Hence, more molecules near the wall show more negative potential energy and lower pressure.

In addition, as we shown before, the stronger the intermolecular interaction between solid and gas molecules, the solid wall attract more gas molecules, so the contribution of virial part to the more negative relative pressure. As a result, the overall pressure should show a decreasing trend as the interatomic interaction increases. The result is shown in Fig. 5.1(b). In a word, the pressure is dependent on the interaction between solid and gas molecules. In addition, if the solid-gas interaction is low enough in sys2, the final pressure performance should be similar to the pressure profile with ‘WCA’ potential. As to this point, we can explain it by the flow velocity distributions in the channels for different gas-wall interactions [6].

5.2. Density Distribution

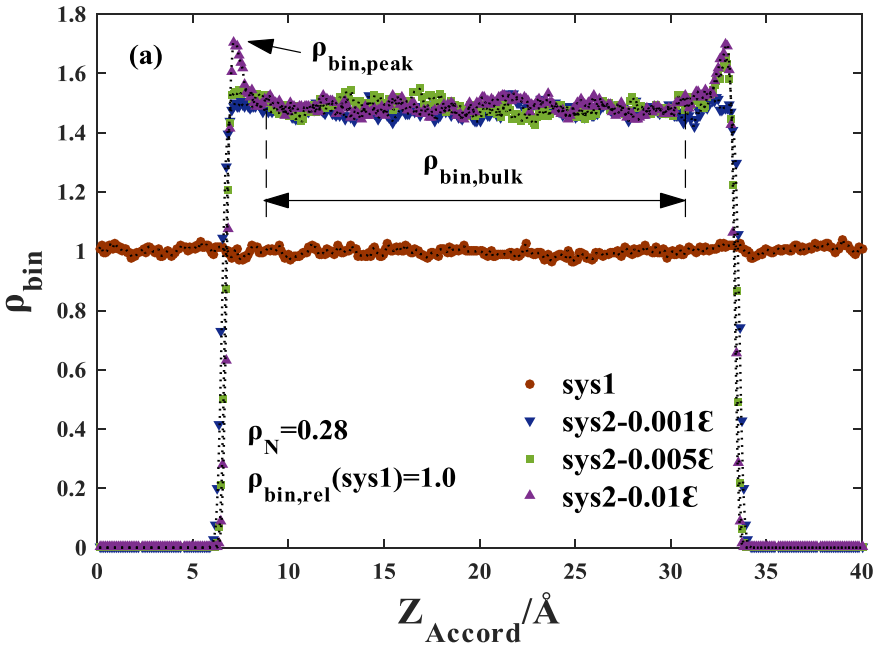
(a)
ρbin,peak
ρbin,bulk
ρbin
ρN=0.28
ρbin,rel(sys1)=1.0
sys1
sys2-0.001Ɛ
sys2-0.005Ɛ
sys2-0.01Ɛ
ZAccord/Å

sys 1

sys 2

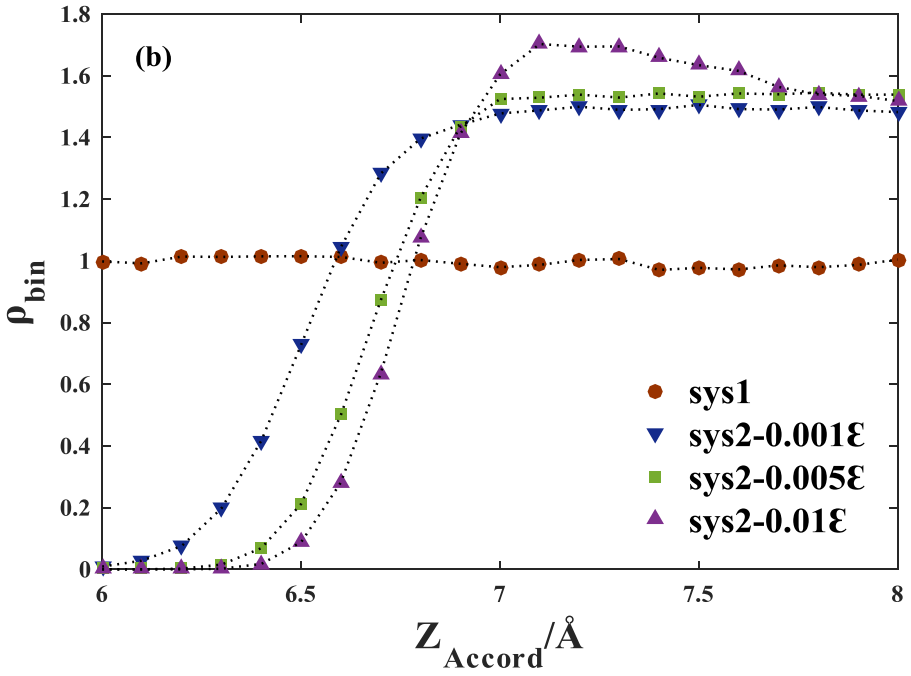

Figure 5.2 The relative number density profile each bin (a) the comparison of number density in sys1 and sys2 with variable interatomic interaction (b) partial magnification of number density in sys2 with variable interaction

In this part, MD simulation was used to investigate the number density each bin in sys1 and sys2 with variable interaction. The bin size is 0.1angstrom. Except the wall in sys2, all of the other environment variables are same. The result's was shown in Fig. 5.2. Here, ρ_{bin} represents the relative number density each bin, it was calculated as the following formula:

$$\rho_{bin} = 400 * Ncount / 97 \tag{5.2}$$

There are a total of 400 bins, the number of simulated gas molecules are 97. In Fig. 5.2(a), the density distribution in sys1 and sys2 were compared. In sys1, there is slightly fluctuating but close to the 1.0.

Moreover, the molecular position is also given in sys1 and sys2. We put a simple model: two-dimensional MD gas flow simulations with the solid wall using the (1,1,0) plane. Due to the systematic error of the missing atoms at the time of MD simulation, we add a gap of 2.08Å between the solid atom region and the gas atom region. And, in the two-dimensional molecular simulation schematic, "~" represents the gap. Therefore, the initial change in the pressure distribution in sys2 (from zero value in first few bins) is later than that in the similar system (0.41~0.47Å). Due to the factor of overlap, there exists any zero number density value near the wall in sys2. And we will explain the atomic overlap in detail in the next section. As to the sys2, the zero value exists in first few bins. However, almost the number density is similar each bin in sys1. Therefore, the average number density is lower than simulation results in sys2. As for sys2, it can be found clearly more gas molecules are gathered close to the solid wall in higher solid-gas interaction. We enlarged this part in detail in Fig. 5.2(b). Thus, the simulation results of average pressure are verified by another way: in bulk field, the number density is approximately same. So the final average pressure value is dominated by the peak data near the solid wall. Except the stronger interactions with the stronger peak density, it can be observed where the number density starts changing from zero value early under weaker gas-solid interaction.

As I have drawn in Fig. 5.2(a), the $\rho_{bin,peak}$ and $\rho_{bin,bulk}$ were defined. It represent the peak number density value near the solid wall and bulk density in relatively stable field respectively. According to the different intermolecular interaction, the number density showed a regular change. Therefore, we analyzed the data and get the Fig. 5.3. Because of the coarse statistical data due to the lack of huge numbers of data, we utilized MATLAB for its curve fitting. The result is shown in below:

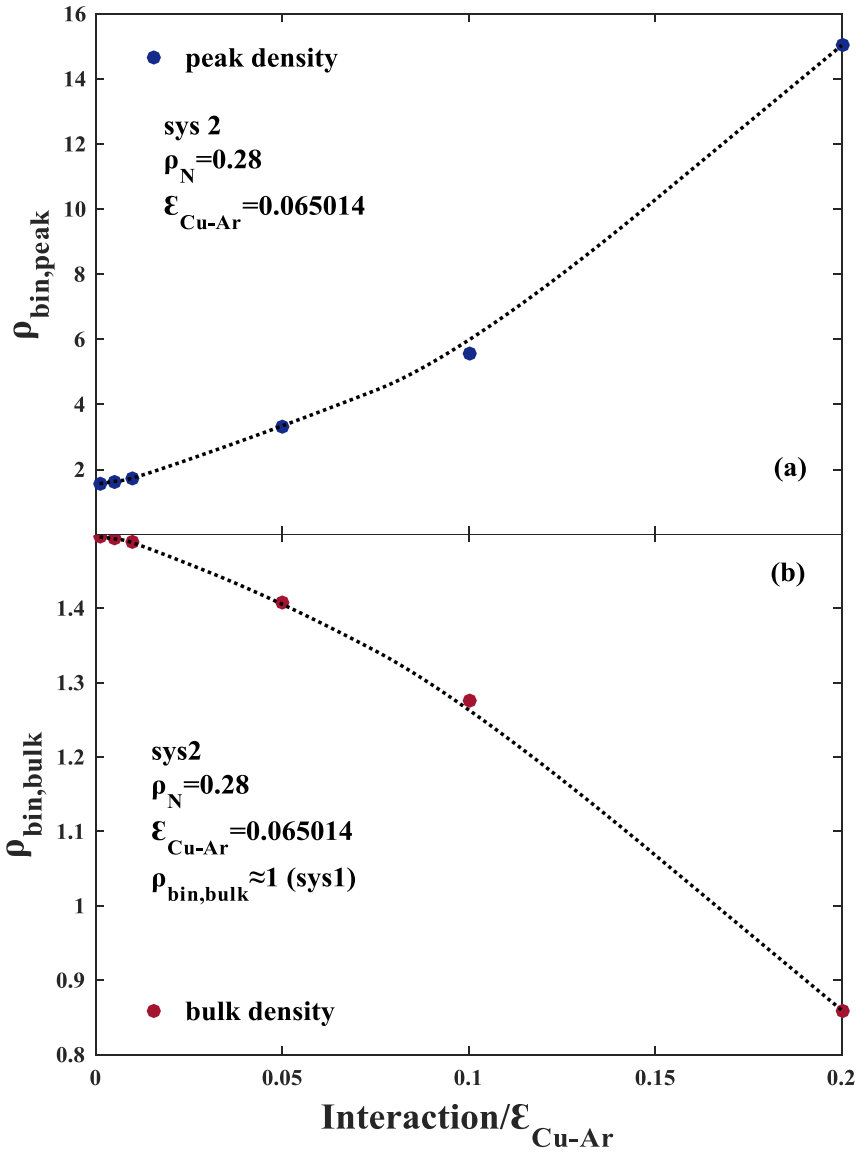

Figure 5.3 The relationship between number density and interatomic interaction (a) peak number density near the solid wall with variable interaction (b) bulk number density in relatively stable field with variable interaction

As shown in previous figures, there are more molecules near the solid wall under higher solid-gas interaction. That is, as the intermolecular interaction increases, the peak number density near the solid wall increases. In addition, within same molecules number, higher peak

density corresponds to lower bulk density. Hence, the result in Fig. 5.3(b) shows the relationship between interaction and bulk number density.

5.3. Pressure Distribution

In this part, MD simulations were used to investigate the pressure distribution in sys1 and sys2. In Fig. 5.4(a), we show the comparison of pressure distribution in sys1 and sys2 with variable interaction. Due to the factor of atomic overlap, the initial change in the pressure distribution in sys2 (from zero value in first few bins) is zero value. The general pressure distribution is shown in Fig. 5.4(a). In sys1, the gas molecules are free to move in a virtual box with periodic boundaries. Therefore, the pressure each bin is almost same, so the relative pressure $\Pr \approx 4.3109 kPa$ as shown in figure. In Fig. 5.4(b), we could observe clearly the pressure distribution under different interaction in detail. Except the stronger interactions with the stronger peak value of local pressure, it can be concluded the weaker interaction is, the earlier position the pressure starts to change from zero value.

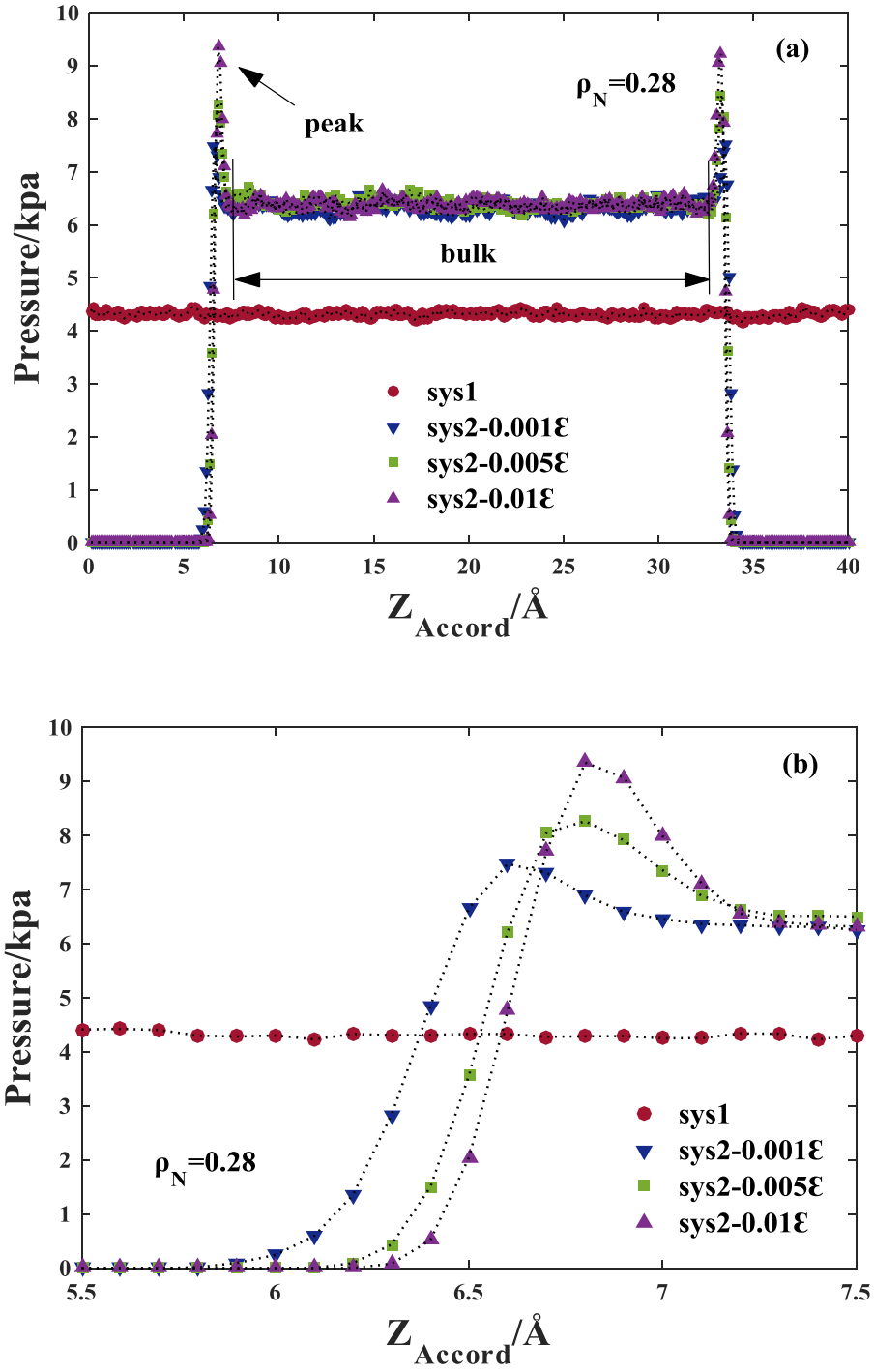

Figure 5.4(a) The pressure distribution in sys1 and sys2 with variable interaction and two-dimensional MD gas flow simulations with the solid wall using the (1,1,0) plane (b) The partial magnification of pressure distribution each bin in sys1 and sys2

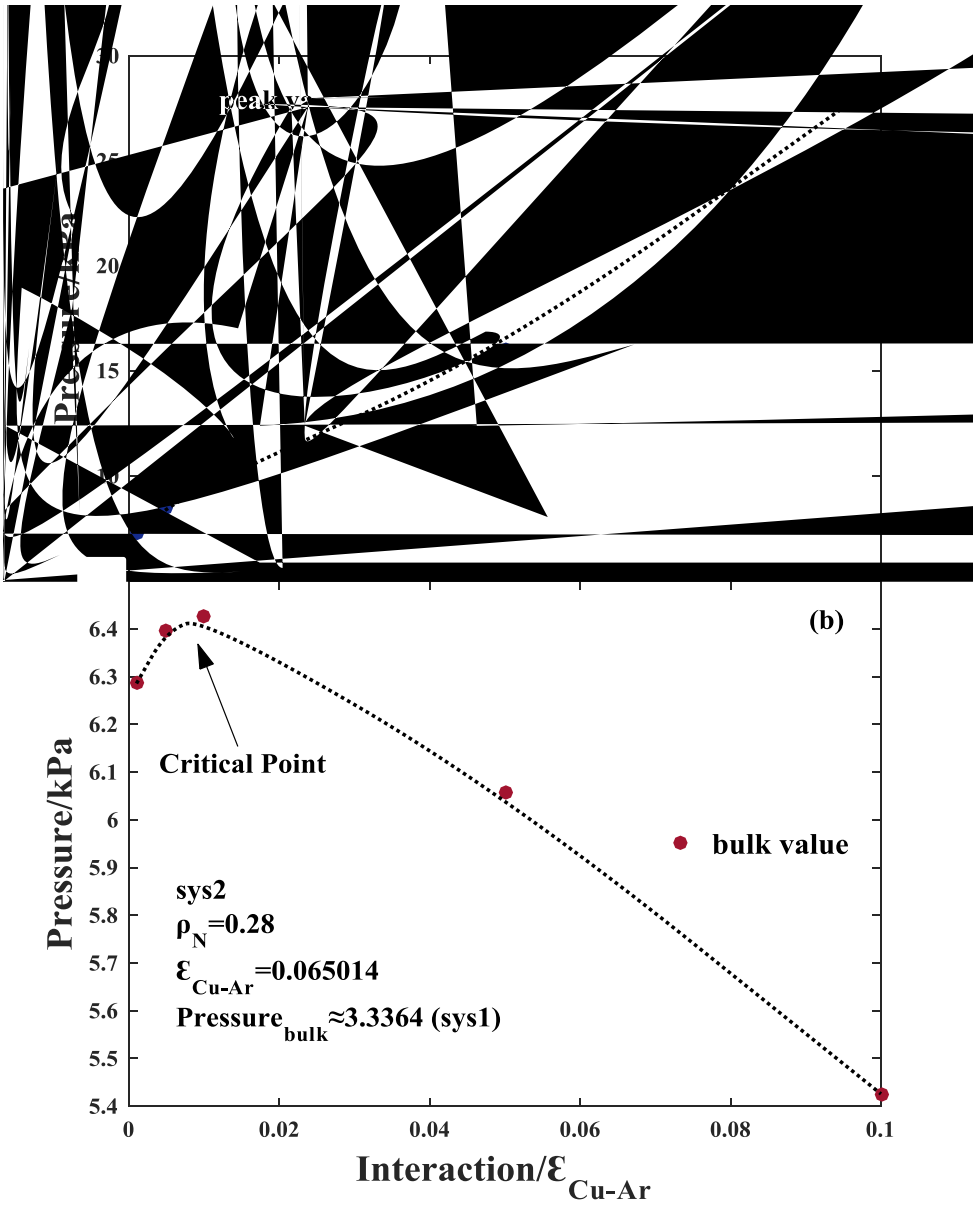

Figure 5.5 The relationship between pressure and interatomic interaction (a) peak pressure value near the solid wall under variable interaction (b) bulk pressure in relatively stable field with variable interaction

In the Fig. 5.5(a), as we know, the pressure consists of kinetic and virial parts. And near the solid wall, the gas molecules have higher kinetic energy and virial energy contribution for the local pressure in the stronger solid-gas interaction. Thus, the peak pressure tends to increase with the increasing interaction. However, as to bulk pressure value, the situation becomes complicated

due to the pressure contribution of two components with different trends. From the previous results in Fig. 4.3, it can be found that the virial energy contribution for pressure will appear more obvious negative as increasing solid-gas interaction, while the kinetic energy is increased due to the increasing number density of gas molecules near the solid wall. So there is a critical point. Compared the pressure components with 0.001ε and 0.01ε solid-gas interaction, the bulk local pressure on kinetic term is decreasing as the increasing interaction, and the virial term contribution in the bulk region should have been decreased. However, there exists the negative value after the positive peak value for virial term as shown in Fig. 4.3. And this part of negative contribution of virial term will be calculated in the bulk pressure since the overall pressure distribution tends to be stable when the interaction is small enough. Therefore, in order to balance this part of the negative pressure contribution, the bulk pressure of virial term should be increased when the solid-gas interaction is smaller relatively. In other words, this relatively small interaction value is before the critical point. And after this critical point, the negative peak value of viral term can be observed clearly, and some of them are calculated into the overall bulk pressure. At the same time, it was considered that the kinetic term on the bulk pressure has also made a contribution to reduce. So, the overall bulk pressure decreased as increasing the interaction.

CHAPTER VI

CONCLUSIONS

In this thesis, I focus on investigating the gas pressure in virtual box with or without wall. In particular, I employ equilibrium molecular dynamics simulations using LAMMPS to study gas pressure confined between two parallel solid walls.

In Chapter III, we conducted a series of MD simulation methods of pressure on gas in different systems, nanochannel and virtual cubes under the same environment parameters. Also, we showed the calculation method of gas pressure by numerical analysis, IK pressure expression. This expression was used to compute the stress tensor components and can be derivate by the Virial Theorem. Through this IK expression, we can clearly understand the components of gas pressure. One term is related to the ideal gas law and it was calculated by considering the momentum resulting from the particle velocities, whereas the particle-particle virial terms are corrections to the ideal gas law because of the interaction of particles having non-zero volumes and forces fields.

In Chapter IV, through the Radial Distribution Function (RDF), we can distinguish the state of the fluid in simulation system. So, the results showed that the simulated fluid is gas and the simulation result is valid measurement. In addition, two simulation methods, directly (‘compute stress’) and indirectly (‘compute ks + vs’), were compared with the experiment data (NIST). Except the deviation caused by the intermolecular potential type (little deviation ratio), it is feasible to use MD simulation results to compare with the calculation by IGL. And the difference between simulation and calculation results increases with the increasing the number density due to the more and more non-negligible atomic volume. Beyond that, virial and kinetic

contributions on pressure under different gas-solid interaction were simulated to investigate the relationship among them. The pressure value is constant in the bulk region, while the surface virial only has a significant effect on the pressure near the wall. Therefore, higher gas-solid interaction, more gas molecules were absorbed near the solid wall due to the wall force field. And, it can be concluded that the pressure simulation results are almost same with each other between sys 1 and sys 2 when the pressure tends to be stable in bulk region.

In Chapter V, I dedicated particular attention to comparison in fluid density and pressure distribution. Variable weaker interaction between solid and gas molecules were used to investigate the density and pressure. Also, the results of sys1 and sys2 are compared. Through the analysis and summary of simulation data, the results are as follows:

(1) Due to the wall force field of solid wall, there is a significant difference in average pressure profile for the presence of solid walls (between sys 1 and sys 2). As a result, because stronger gas-solid interaction can attract more gas molecules, the overall pressure should show a decreasing trend as the interatomic interaction increases. In a word, the pressure is dependent on the interaction between solid and gas molecules. In addition, combined with the results of the previous chapter, different from the virial part of negative value in traditional simulation method, the virial part is positive and close to zero due to the composing only by the repulsive potential in WCA simulation method. The results show that the gas pressure tends to be that with WCA potential when the gas-solid interaction is weaker enough.

(2) It can be considered that this difference of number density occurs only near the solid wall. As to sys2, it can be found clearly more gas molecules are gathered close to the solid wall in higher solid-gas interaction. Considering the factor of molecular overlap, there is a little difference in

bulk field between sys 1 and sys 2. Thus, the simulation results of average pressure in last result are verified by another way: in bulk field, the number density is approximately same; the final average pressure value is dominated by the peak data near the solid wall. That is, as the intermolecular interaction increases, the peak number density near the solid wall increases, and higher peak density corresponds to lower bulk density.

(3) Except the stronger interactions with the stronger peak value of local pressure, it can be concluded that weaker gas-solid interaction is, the pressure starts changing from zero value earlier. And same with the previous one, the peak pressure tends to increase and bulk pressure tends to decrease with the increasing interaction.

Overall, the nanoscale model of the virtual box with or without solid wall is significant on the gas behavior, especially pressure, due to the surface force field and intermolecular interaction. Also, these results in this work can be applied to more other research about the gas behavior with kinds of solid walls as long as the same intermolecular interaction between solid and gas molecules and the same crystal structure.

REFERENCE

[1]. C. Cercignani and M. Lampis. Kinetic models for gas-surface interactions. Transport Theory and Statistical Physics 1, 101-114 (1971)

[2]. P. M. Agrawal, B. M. Rice, and D. L. Thompson. Predicting Trends in Rate Parameters for Self-diffusion on FCC Metal Surfaces. Surface Science 515, 21 (2002)

[3]. Ali Beskok, and Murat Barisik. Molecular Dynamics Studies on Nanoscale Gas Transport. Encyclopedia of Microfluidics and Nanofluidics, 2307-0315(2014)

[4]. Karniadakis, G., Beskok, A. and Alulu, N. Simple Fluids in Nanochannels. Springer New York, 365-406(2005)

[5]. Truong Quoc Vo, and BoHung Kim. Transport Phenomena of Water in Molecular Fluidic Channels. Scientific Reports 6, 33881 (2016)

[6]. A. J. Markvoort and P. Ajhilbers. Molecular dynamics study of the influence of wall-gas interactions on heat flow in nanochannels. Physical Review E 71, 066702 (2005)

[7]. Moran Wang, Xudong Lan and Zhixin Li. Analyses of Gas Flows in Micro- and Nanochannels. International Journal of Heat and Mass Transfer 51, 3630-3641(2008)

[8]. Michael Frank, Dimitris Drikakis and Nikolaos Asproulis. Thermal Conductivity of Nanofluid in Nanochannels. Microfluid Nanofluid 19, 1011-1017(2015)

[9]. Joe Francis Thekkethala and Sarith P. Sa. The effect of graphene layers on interfacial thermal resistance in composite nanochannels with flow. Microfluid Nano-fluid 18, 637-648(2015)

[10]. Murat Barisik and Ali Beskok. Equilibrium molecular dynamics studies on nanoscale-confined fluids. Microfluid Nano-fluid 11, 269-282(2011)

[11]. Youngkyun Jung. Velocity inversion in nanochannel flow. Physical Physics E 75, 051203(2007)

[12]. Jafar Ghorbanian and Ali Beskok. Scale effects in nano‐channel liquid flows. Microfluid Nanofluid 20, (2016)

[13]. An Pham, Murat Barisik and BoHung Kim. Pressure dependence of Kapitza resistance at gold/water and silicon/water interfaces. The Journal of Chemical Physics 139, 244702(2013)

[14]. Nikolaos Asproulis and Dimitris Drikakis. Boundary slip dependency on surface stiffness. Physical Review E 81, 061503(2010)

[15]. Shigeo Maruyama and Tatsuto Kimura. A Study on Thermal Resistance over a Solid-Liquid Interface by the Molecular Dynamics Method. Thermal Science & Engineering 7, 63-68(1999)

[16]. Murat Barisik, Bohung Kim and Ali Beskok. Smart Wall Model for Molecular Dynamics Simulations of Nanoscale Gas Flows. Commun. Comput. Phys 7, 977-993(2010)

[17]. Murat Barisik and Ali Beskok. Molecular Dynamics simulations of Shear-driven Gas Flows in Nano-channels. Microfluid Nanofluid 11, 611-622(2011)

[18]. J.H. Kim, A.J. Frijns and A. van Steenhoven. Pressure Calculations in Nanochannel Gas Flows. Journal of Physics 362, 012020(2012)

[19]. Peter A. Thompson and Sandra M. Troian. A general boundary condition for liquid flow at solid surfaces. Letters to Nature 389, 360-362(1997)

[20]. Jaime Wisniak. Heike Kamerlingh: The Virial Equation of State. Indian Journal of Chemical Technology 10, 564-572(2003)

[21]. Fubing Bao and Yuanlin Huang. Investigation of pressure‐driven gas flows in nanoscale channels using molecular dynamics simulation. Microfluid and Nanofluid 18, 1075-1084(2015)

[22]. Hendrik Heinz, Wolfgang Paul and Kurt Binder. Calculation of Local Pressure Tensors in Systems with Many-Body Interactions. Phys. Rev. E 72, 066704(2003)

[23]. Bohung Kim, Ali Beskok and Tahir Cagin. Thermal interactions in nanoscale fluid flow: molecular dynamics simulations with solid–liquid interfaces. Microfluidics and Nanofluidics 5, 551-559 (2008)

[24]. J Toth. Adsorption: theory modeling and analysis. Marcel Dekker 107, New York (2005)

[25]. Alexander Stukowski. Visualization and analysis of atomistic simulation data with OVITO–the Open Visualization Tool. Modelling and Simulation Materials Science Engineering 18, 015012(2009)

[26]. Michael L. Parks, Pablo Seleson, Steven J. Plimpton, Stewart A. Silling and

Richard B. Lehoucq. Peridynamics with LAMMPS: A User Guide v0.3 Beta. Sandia Report, (2011)

[27]. Mei, J., Davenport, J. W., and Fernando, G. W. Analytic Embedded-Atom Potentials for FCC Metals: Application to Liquid and Solid Copper. Physical Review B 43, 4653-4658 (1991)

[*28*]. M. J. Madou, Fundamentals of microfabrication: the science of miniaturization, 2nd ed. CRC Press, Boca raton, FL, 2002.

[29]. C. M. Ho and Y.-C. Tai, Micro-electro-mechanical-system(MEMS) and fluid flows, Annu. Rev. Fluid Mech., 30, 579-612, 1998.

[30]. M. Gad-el-Hak, the fluid mechanics of micro-devices: the freeman scholar lecture, J. Fluids Engi., 121, 5-33, 1999.

[31]. Burcu Gumuscu, Compartmentalized 3D Tissue Culture Arrays under Controlled Microfluidic Delivery, Scientific Reports, 2017.

[32]. Bakil, C. and Chakraborty, S. Capillary filling dynamics of water in nanopores. Applied Physics Letters 101, 153112(2012).

[33]. H.-S. Tsien. Superaerodynamics, Mechanics of Rarefied Gases. Journal of the Aeronautical Science 13, 653-664(1946).

[34]. Van Noorden, R. Modelers react to chemistry award: prize proves that theorists can measure up to experimenters. Nature 502, 7471(2013).

[35]. Plimpton, S. Fast parallel algorithms for short-range molecular dynamics. Journal of Computational Physics 117, 1-19 (1995).

[36]. Allen, M. P. and Tildesley, D. J., 1989. Computer simulations of liquids.

[37]. G. A. Bird, 1994. Molecular gas dynamics and the direct simulation of gas flows.

[38]. D. Poulikakos, S. Arcidiacono and S. Maruyama, 2003. Molecular dynamics simulation in nanoscale heat transfer.

[39]. Richard. Sadus. Simple equation of state for hard-sphere chains. AIChE Journal 45, 2454-2457 (1999).

[40]. George Karniadakis, Ali Beskok and Narayan Aluru. Microflows and nanoflows: fundamentals and simulations (2006).

[41]. Carl Y. H. Jiang, A New Approach to Model Adsorption in Heterogeneous Phase System. American Journal of Materials Science 4, 25-38 (2014).

[42]. J. H. Irving and J. G. Kirkwood, J. Chem. Phys. 18, 917(1950).

[43]. TQ Vo and BH Kim. Near-surface viscosity effects on capillary rise of water in nanotubes. Physical Review E 92, 053009(2015).

[44]. M. Gad-el-Hak. The fluid mechanics of microdevices—the freeman scholar lecture. J. Fluids Eng 121(1), 5-33(1999)

[45]. Murat Barisik and Ali Beskok. "Law of the nano‐wall" in nano‐channel gas flows. Microfluid Nanofluid, (2016)

[46]. Ning Yu and Andreas A. Polycarpou. Adhesive contact based on the Lennard–Jones potential: a correction to the value of the equilibrium distance as used in the potential. Journal of Colloid and Interface Science 278, 428-435(2004)

[47]. Zhi Liang and Hai-Lung Tsai. Thermal conductivity of interfacial layers in nanofluids. Physical Review E 83, 041602(2011)

[48]. Truong Quoc Vo and BoHung Kim. Interface Thermal Resistance between Liquid Water and Various Metallic Surfaces. International journal of Precision and Manufacturing 16, 1341-1346(2015)

[49]. Murat Barisik and Ali Beskok. Molecular free paths in nanoscale gas flows. Microfluid nanofluid 18, 1365-1371(2015)

[50]. J. L. Yarnell, M. J. Katz and R. G. Wenzel. Structure factor and Radial Distribution function for liquid argon at 85 K. Physical review A 7, 2130-2144(1973)

[51]. Timothée Ewart, Pierre Perrier, Irina Graur, Jean-Luc Firpo, J. Gilbert Méolans and David Zeitoun. Tangential momentum accommodation coefficient in a microtube. 18 Congres Francais de mecanique, 27-31(2007)

[52]. T. Avanessian and g. Hwang. Thermal diode in gas-filled nanogap with heterogeneous surfaces using nonequilibrium molecular dynamics simulation. Journal of Applid Physics 120, 165306(2016)

[53]. Francois Detcheverry and Lyd´eric Bocquet. Thermal fluctuations of hydrodynamic flows in nanochannels. Physical Review E 88, 012106(2013)

[54]. Frank Schreiber, Fabio Zanini and Felix Roosen-Runge. Virial expansion-a brief introduction. (2011)

[55]. G. C. Sih. Use specification of multiscale materials for life spanned over macro-, micro-, nano-, and pico-scale. Theoretical and Applied Fracture Mechanics 53, 94-112(2011)

[56]. Shiang-Tai Lin, Mario Blanco, and William A. Goddard III. The two-phase model for calculating thermodynamic properties of liquids from molecular dynamics: Validation for the phase diagram of Lennard-Jones fluids. The Journal of Chemical Physics 119, 11792(2003)